

Article

# Phase Stability and Transport Properties of $(\text{ZrO}_2)_{0.91-x}(\text{Sc}_2\text{O}_3)_{0.09}(\text{Yb}_2\text{O}_3)_x$ Crystals ( $x = 0-0.01$ )

Mikhail Borik<sup>1</sup>, Galina Korableva<sup>2</sup>, Alexey Kulebyakin<sup>1,\*</sup>, Irina Kuritsyna<sup>2</sup>, Nataliya Larina<sup>3</sup>, Elena Lomonova<sup>1</sup>, Filipp Milovich<sup>1,4</sup>, Valentina Myzina<sup>1</sup>, Polina Ryabochkina<sup>3</sup>, Nataliya Sidorova<sup>3</sup>, Nataliya Tabachkova<sup>1,4</sup> and Tatyana Volkova<sup>3</sup>

<sup>1</sup> Prokhorov General Physics Institute of the Russian Academy of Sciences, 38 Vavilov str., 119991 Moscow, Russia; borik@lst.gpi.ru (M.B.); lomonova@lst.gpi.ru (E.L.); philippmilovich@gmail.com (F.M.); vamyzina@lst.gpi.ru (V.M.); ntabachkova@gmail.com (N.T.)

<sup>2</sup> Institute of Solid State Physics of the Russian Academy of Sciences, 2 Academician Osip'yan str., 142432 Chernogolovka, Moscow District, Russia; eliseevagm@mail.ru (G.K.); koneva@issp.ac.ru (I.K.)

<sup>3</sup> Institute of Physics and Chemistry, National Research Mordovia State University, 68 Bolshevistskaya str., 430005 Saransk, Republic of Mordovia, Russia; saharova.1996@mail.ru (N.L.); Ryabochkina@freemail.mrsu.ru (P.R.); ya.natalka2112@yandex.ru (N.S.); sendboxvv@mail.ru (T.V.)

<sup>4</sup> Department of Materials Science of Semiconductors and Dielectrics, National University of Science and Technology (MISIS), 4 Leninskiy prospekt, 119049 Moscow, Russia

\* Correspondence: kulebyakin@lst.gpi.ru

**Abstract:** Phase stability and transport properties of  $(\text{ZrO}_2)_{0.91-x}(\text{Sc}_2\text{O}_3)_{0.09}(\text{Yb}_2\text{O}_3)_x$  crystals ( $x = 0-0.01$ ) have been studied before and after air annealing at 1000 °C for 400 h. The crystals have been grown by radio frequency (RF) heating in a cold crucible. The microstructure, phase composition, and electrical conductivity of the crystals have been studied using optical microscopy, X-ray diffraction, Raman spectroscopy, and impedance spectroscopy. Phase stability and degradation of ionic conductivity of the crystals upon long-term high-temperature heat treatment have been discussed. We show that the stabilization of  $\text{ZrO}_2$  co-doped with 9 mol.%  $\text{Sc}_2\text{O}_3$  and 1 mol.%  $\text{Yb}_2\text{O}_3$  provides transparent uniform crystals with the pseudocubic  $t''$  phase structure having high phase stability. Crystals of this composition had the highest conductivity in the entire temperature range. Long-term high-temperature annealing of these crystals did not lead to conductivity degradation.

**Keywords:** directional melt crystallization; skull melting; single crystal; zirconia; scandia; dielectric materials; solid electrolytes; ionic conductors



**Citation:** Borik, M.; Korableva, G.; Kulebyakin, A.; Kuritsyna, I.; Larina, N.; Lomonova, E.; Milovich, F.; Myzina, V.; Ryabochkina, P.; Sidorova, N.; et al. Phase Stability and Transport Properties of  $(\text{ZrO}_2)_{0.91-x}(\text{Sc}_2\text{O}_3)_{0.09}(\text{Yb}_2\text{O}_3)_x$  Crystals ( $x = 0-0.01$ ). *Crystals* **2021**, *11*, 83. <https://doi.org/10.3390/cryst11020083>

Received: 10 December 2020

Accepted: 14 January 2021

Published: 21 January 2021

**Publisher's Note:** MDPI stays neutral with regard to jurisdictional claims in published maps and institutional affiliations.



**Copyright:** © 2021 by the authors. Licensee MDPI, Basel, Switzerland. This article is an open access article distributed under the terms and conditions of the Creative Commons Attribution (CC BY) license (<https://creativecommons.org/licenses/by/4.0/>).

## 1. Introduction

The use of stabilizing scandium oxide in zirconia based solid electrolytes provides high ionic conductivity material. Electrolytic membranes of these materials significantly reduce the working temperature of the electrochemical devices while retaining their high electrical conductivity, which is of high importance for service life and reliability of electrochemical reactors, solid oxide fuel cells, electrolyzers, and sensors [1–5].

Polycrystalline ceramic materials are typically used in these devices. Ceramic technologies impose only little limitations on the shape and dimensions of final devices. However, zirconia based ceramic solid state electrolytes obtained using different methods exhibit quite different electrical conductivities [6–10]. This difference has been reported to originate from differences in the microstructure, impurity content, and thermal history of the materials, arising from technological aspects.

Zirconia based materials can be produced using not only ceramic technologies, but also directional melt crystallization [11,12]. This method is characterized by high productivity and makes it possible to obtain up to several hundred kilograms of single crystals in one technological cycle (24 h). The cold crucible design does not require any special devices limiting the number of grown crystals, e.g., devices used in hot crucibles. Directional melt

crystallization process produces an ingot consisting of multiple columnar single crystals whose number and sizes depend on growth process parameters. Another advantage of this method is the fast in-melt synthesis from the raw oxides, which does not require any intermediate or preliminary stages at which the raw materials might be contaminated. The high melting points ( $\sim 3000$  °C) accelerate the removal of volatile impurities from the melt. Furthermore, directional melt crystallization removes a number of impurities, e.g., silicon, aluminum, titanium, tungsten, molybdenum, etc., which are displaced during directional crystallization because their distribution coefficients in zirconia are less than 1 [12]. The conductivity of crystals grown by directional melt crystallization only depends on the initial composition and crystallization conditions, unlike for materials obtained using ceramic technologies.

Different authors reported that solid solutions with the composition  $\text{ZrO}_2 - (9-10)$  mol.%  $\text{Sc}_2\text{O}_3$  have the highest ionic conductivity [13–17]. However, the structural and electrical properties of these materials are very sensitive to the  $\text{Sc}_2\text{O}_3$  content [13,18]. For example, it was reported [18] that ceramics with 9.3 mol.%  $\text{Sc}_2\text{O}_3$  has the highest ionic conductivity whereas above 9.5 mol.%  $\text{Sc}_2\text{O}_3$  the rhombohedral phase forms and coexists with the cubic phase at room temperature. In comparison with the cubic phase, the rhombohedral phase has a low conductivity. Upon heating, the rhombohedral phase transforms to the cubic phase in the temperature range 400 to 600 °C. For scandia stabilized zirconia the phase boundaries have been determined only approximately, because metastable phases exist in this system and, therefore, the phase composition of the material depends on its synthesis method and conditions.

An important problem limiting the use of  $\text{ZrO}_2\text{-Sc}_2\text{O}_3$  solid solutions as solid electrolytes is the instability of the transport characteristics of the material during long-term device operation. The reasons for this behavior of conductivity in this system have been studied in a number of articles [19–22]. The instability originates from the metastability and multiphase composition of the materials causing phase transformations of the most conducting compositions at operation temperatures and, hence, reduction of oxygen-ionic conductivity of the materials. One method to provide stable phase composition and transport properties is additional doping of the  $\text{ZrO}_2\text{-Sc}_2\text{O}_3$  solid solution with rare earth oxides which favor the formation of single-phase solid solutions that are stable at solid state electrolyte operation temperatures [23]. This additional doping should not lead to a noticeable decrease in the conductivity of the material. The  $\text{Yb}_2\text{O}_3$  is one of the promising oxides that stabilize the cubic phase in  $\text{ZrO}_2\text{-Sc}_2\text{O}_3$  solid solutions. Currently, there is interest in studying the structure and transport characteristics of ceramic and crystalline samples of  $\text{ZrO}_2\text{-Sc}_2\text{O}_3$  solid solutions additionally doped with  $\text{Yb}_2\text{O}_3$  [24–26]. The effect of long-term annealing at 650 °C in air on the properties of  $\text{ZrO}_2$  solid solutions containing 8–9 mol%  $\text{Sc}_2\text{O}_3$  and additionally co-doped with 1 mol%  $\text{Yb}_2\text{O}_3$  has been studied [27]. It was shown that the introduction of 1 mol%  $\text{Yb}_2\text{O}_3$  reduces the degradation of the conductivity of  $\text{ZrO}_2\text{-Sc}_2\text{O}_3$  solid solutions. However, since the operating temperatures of  $\text{ZrO}_2$ -based solid electrolytes are  $\sim 900$  °C, it is of interest to study the structural and electrophysical characteristics of  $\text{ZrO}_2\text{-Sc}_2\text{O}_3$  solid solution samples additionally stabilized with  $\text{Yb}_2\text{O}_3$ , which were subjected to heat treatment at higher temperatures.

The aim of this work is to study the effect of long-term annealing (at a temperature of 1000 °C for 400 h) on the phase composition and conductivity of  $(\text{ZrO}_2)_{0.91-x}(\text{Sc}_2\text{O}_3)_{0.09}(\text{Yb}_2\text{O}_3)_x$  crystals.

## 2. Materials and Methods

The  $(\text{ZrO}_2)_{0.91-x}(\text{Sc}_2\text{O}_3)_{0.09}(\text{Yb}_2\text{O}_3)_x$  solid solution single crystals where  $x = (0; 0.005; 0.01)$  were synthesized using directional melt crystallization in a cold crucible. The raw materials were high purity powdered zirconia, scandia and ytterbia containing at least 99.96 wt.% of the respective materials. The raw materials were mechanically mixed, loaded into a water-cooled tube container and melted by direct RF heating. The RF generator

frequency was 5.28 MHz and its power was 60 kW. Metal zirconium was used for initial melting. Melt crystallization in a cold skull produced an ingot consisting of single crystals.

The as-grown crystals were heat treated at 1000 °C in air for 400 h in an HT 04/16.2 high-temperature furnace.

The phase composition of the crystals was analyzed by X-ray diffraction on a Bruker D8 diffractometer in CuK $\alpha$  radiation and using Raman spectroscopy with a 633 nm excitation laser. The density of the crystals was measured by hydrostatic weighing on a Sartorius instrument. The microstructure of the specimens was studied for 1.5 mm thick plane-parallel wafers cut along the crystal growth axis using polarized transmitted light optical microscopy under a Carl Zeiss Axio Imager Z2 microscope.

The conductivity of the crystals was studied at 300–900 °C using a Solartron SI 1260 frequency analyzer in the 1 Hz–5 MHz frequency range with an alternating current signal amplitude of 24 mV. The test wafers were 7 × 7 mm<sup>2</sup> squares 0.5 mm in thickness. The current contacts were formed on opposite sides of the crystals from platinum paste annealed at 950 °C in air for 1 h. The impedance spectra were processed with the ZView version 2.8 software. The conductivity of the crystals was calculated from the impedance spectra processing data taking into account the specimen dimensions.

### 3. Results and Discussion

The ZrO<sub>2</sub> crystals grown using directional melt crystallization in a cold crucible and stabilized with 9 mol.% Sc<sub>2</sub>O<sub>3</sub> and additionally doped with 0.5 mol.% Yb<sub>2</sub>O<sub>3</sub> and 1 mol.% Yb<sub>2</sub>O<sub>3</sub> are hereinafter denoted as 9ScSZ, 9Sc0.5YbSZ and 9Sc1YbSZ. The cross-section sizes of the crystals were 10 to 15 mm and their lengths were 30 to 45 mm. Figure 1 shows polarized light microstructure images of wafers cut from the crystals along the growth axis.

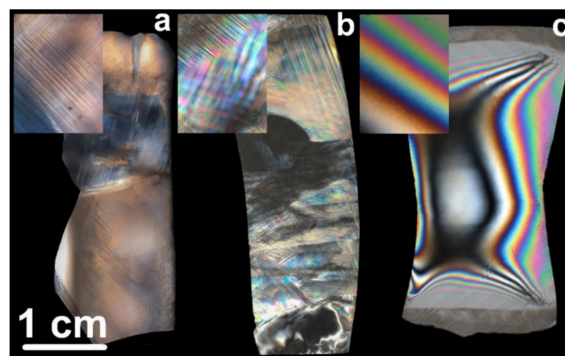


**Figure 1.** Polarized light microstructure images of as-grown crystals: (a) 9ScSZ, (b) 9Sc0.5YbSZ, and (c) 9Sc1YbSZ.

The as-grown 9ScSZ crystals were completely semitransparent and contained no cracks. The microstructure images of the crystals show elongated structural features which have different orientations in different crystal regions. This crystal microstructure is produced by transformation twins forming upon crystal cooling. There are several options of the ZrO<sub>2</sub>-Sc<sub>2</sub>O<sub>3</sub> phase diagram which differ considerably, the differences being the greatest in the region of ZrO<sub>2</sub>-9 mol.% Sc<sub>2</sub>O<sub>3</sub> composition. The equilibrium room temperature phase composition has not yet been determined authentically, but the phase diagrams suggest that the cubic phase may undergo transitions to the tetragonal and/or rhombohedral phases upon cooling [28,29]. The phase transition from the high-temperature cubic phase which exists at temperatures close to the crystallization point to the tetragonal phase or the rhombohedral phase during cooling of single crystals is accompanied by twinning which reduces the stress generated during the phase transition. Upon annealing, the sizes of the structural features observed in the 9ScSZ crystals became larger, and the boundaries between crystal regions with different structures became clearer. The as-annealed 9ScSZ crystals contained microcracks.

Addition of 0.5 mol.%  $\text{Yb}_2\text{O}_3$  to the 9ScSZ solid solution produced discrete transparent regions in the crystals. The bottom part of the 9Sc0.5YbSZ crystal, i.e., the part from which crystallization began, contained a uniform transparent region. The middle part of the crystal had a fine twin structure with discrete inclusions of small transparent regions. The top part of the crystal contained large twins that crossed in different directions. The structure of the as-annealed crystals did not contain discrete transparent regions. The microstructure of the 9Sc0.5YbSZ crystals became similar to that of the 9ScSZ crystals. The as-annealed 9Sc0.5YbSZ crystals were uniform and semitransparent and exhibited strong light scattering.

Addition of 1 mol.%  $\text{Yb}_2\text{O}_3$  to the 9ScSZ solid solution produced uniform transparent single crystals. The polarized light microstructure images of the 9Sc1YbSZ crystals exhibit an interference pattern caused by residual growth thermal stress in the crystals. Annealing of the crystals at 1000 °C did not relieve the residual thermal stress but the crystal remained transparent and contained no twins in the bulk.

The phase composition of the crystals was studied using X-ray diffraction for wafers cut from different crystal parts perpendicularly to the  $\langle 100 \rangle$  direction. Table 1 shows data on the phase composition and density of the as-grown and the as-annealed crystals.

**Table 1.** Phase composition, lattice parameters and density of  $(\text{ZrO}_2)_{0.91-x}(\text{Sc}_2\text{O}_3)_{0.09}(\text{Yb}_2\text{O}_3)_x$  crystals before and after annealing at 1000 °C for 400 h.

Sample	As-Grown			As-Annealed		
	Phase *	Lattice Parameters, nm	Density, $\text{g/cm}^3$	Phase	Lattice Parameters, nm	Density, $\text{g/cm}^3$
9ScSZ	t	a = 0.3595(1); c = 0.5122(1)	5.786(3)	t	a = 0.3596(1); c = 0.5124(1)	5.783(3)
				r	a = 0.3559(2); c = 0.9007(2)	
9Sc0.5YbSZ	t	a = 0.3597(1); c = 0.5106(1)	5.816(3)	t	a = 0.3597(1); c = 0.5110(1)	5.818(3)
	c	a = 0.5092(1)				
9Sc1YbSZ	c	a = 0.5094(1)	5.863(3)	c	a = 0.5094(1)	5.862(3)

\* t, c and r are tetragonal, cubic, and rhombohedral modifications of scandia-stabilized zirconia.

The as-grown 9ScSZ crystals were tetragonal according to X-ray diffraction data. The as-annealed 9ScSZ crystals contained two phases: tetragonal and rhombohedral. The growth of the tetragonal phase in the as-annealed crystals testifies to an unstable phase composition of the  $\text{ZrO}_2$  based solid solution if  $\text{Sc}_2\text{O}_3$  is the only doping impurity.

The as-grown crystals co-doped with 0.5 mol.%  $\text{Yb}_2\text{O}_3$  were mixtures of the tetragonal and cubic zirconia modifications. In the tetragonal phase of the 9Sc0.5YbSZ crystal the lattice parameter  $a$  increased and the lattice parameter  $c$  decreased as compared with the respective lattice parameters of the tetragonal phase of the 9ScSZ crystal. The tetragonality degrees of the t phase were 1.007 and 1.004 for the 9ScSZ and 9Sc0.5YbSZ crystals, respectively. The addition of 0.5 mol.%  $\text{Yb}_2\text{O}_3$  to the 9ScSZ solid solution not only changed the lattice parameters of the tetragonal phase but also stabilized the cubic phase in some regions of the crystal. However, the cubic phase in these regions is unstable and transformed to the more stable tetragonal phase upon annealing. In the as-annealed 9Sc0.5YbSZ crystal the lattice parameter  $a$  of the tetragonal phase did not change whereas the lattice parameter  $c$  increased, indicating a shift of the oxygen atoms along the C axis.

The 9Sc1YbSZ crystals contained only the cubic zirconia modification. The phase composition and lattice parameters of the as-annealed cubic zirconia modification did not change.

The density of the crystals depends on the content of stabilizing oxides and on the phase composition of the crystals. The data summarized in Table 1 suggest that co-doping

with  $\text{Yb}_2\text{O}_3$ , which has a higher density ( $9.17 \text{ g/cm}^3$ ) than those of  $\text{ZrO}_2$  ( $5.68 \text{ g/cm}^3$ ) and  $\text{Sc}_2\text{O}_3$  ( $3.86 \text{ g/cm}^3$ ) increases the density of the crystals. The as-annealed 9ScSZ crystal contains rhombohedral phase inclusions, which reduce the density of the crystals, because tetragonal zirconia based solid solution single crystals have the highest density, whereas crystals containing the cubic or rhombohedral phases have lower densities [30]. The density of the as-annealed 9Sc0.5YbSZ crystal increased but slightly, probably also due to the change in the phase composition of the crystals. The density of the as-annealed 9Sc1YbSZ crystals did not change.

We also studied the phase composition of the crystals using Raman spectroscopy. Different from the long-range ordered structure reflected by XRD, the Raman spectrum is sensitive to the short-range ordered structure such as chemical bonds of the internal structure, so it is used to further study the cell distortion [31]. This method reveals even minor changes in the local structure of crystals upon long-term annealing. Figure 2 shows the Raman spectra of the as-grown and as-annealed crystals.

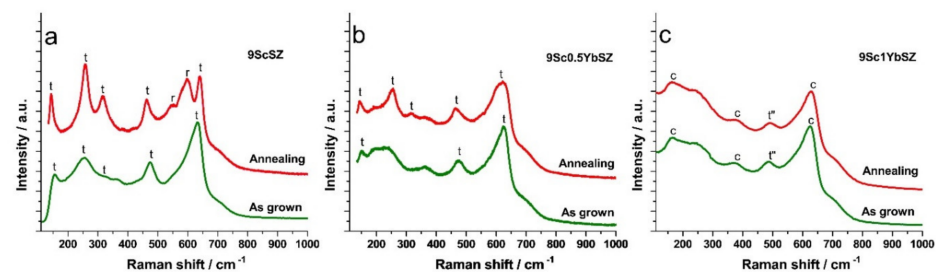


**Figure 2.** Raman spectra of as-grown and as-annealed (a) 9ScSZ, (b) 9Sc0.5YbSZ, and (c) 9Sc1YbSZ crystals.

According to our Raman data the structure of the as-grown 9ScSZ crystals is tetragonal which is indicated by the presence of the typical  $\sim 150 \text{ cm}^{-1}$ ,  $260 \text{ cm}^{-1}$ ,  $470 \text{ cm}^{-1}$ , and  $630 \text{ cm}^{-1}$  bands [32]. However, these bands are quite broadened and shifted toward smaller Raman shift. The Raman spectra of the as-annealed 9ScSZ crystal also contain rhombohedral phase bands [14]. The Raman spectra of the as-grown 9Sc0.5YbSZ crystal are typical of tetragonal structures, but the bands are significantly broadened indicating the presence of the cubic phase along with the tetragonal phase. In the Raman spectra of the as-annealed 9Sc0.5YbSZ crystal, the tetragonal phase bands are clearer. The  $600 \text{ cm}^{-1}$  band is heavily broadened, but does not split in bands typical of the tetragonal and rhombohedral phases as is the case for the as-annealed 9ScSZ crystal.

The spectra of 9Sc1YbSZ crystals exhibits the cubic phase bands and an additional tetragonal phase band near  $\sim 470 \text{ cm}^{-1}$ . According to Raman spectroscopy data, the structure of the 9Sc1YbSZ crystals contains the pseudocubic  $t''$  phase [33,34]. This phase was described as having a degree of tetragonality  $c/a = 1$ , but belonging to the space group of symmetry  $P4_2/nmc$  due to the displacement of oxygen atoms in the anionic sublattice. Thus, according to Raman spectroscopy data, 9Sc1YbSZ crystals are tetragonal ( $t''$  phase), and not cubic, as follows from X-ray diffractometry data. After annealing, the spectrum of 9Sc1YbSZ crystals does not change.

Thus X-ray diffraction and Raman spectroscopy phase composition data suggest that the phase composition of the as-grown 9ScSZ crystals stabilized with only  $\text{Sc}_2\text{O}_3$  is unstable. Annealing causes the formation of the rhombohedral phase along with the tetragonal phase. The crystals contain conjugating phases having different volumes and, therefore, stress accumulating at phase boundaries may fracture the crystals. Co-doping of the  $\text{ZrO}_2 - 9 \text{ mol.}\% \text{ Sc}_2\text{O}_3$  solid solutions with  $0.5 \text{ mol.}\%$  ytterbia stabilizes the high-temperature phase but does not stabilize the cubic phase in the entire crystal. In the 9Sc0.5YbSZ crystals, the co-doping oxide content is insufficient and upon annealing regions with an unstable cubic structure undergo a phase transition to the more stable tetragonal phase, and possibly part of the cubic phase transforms to the rhombohedral phase according to our Raman data.

The pseudocubic  $t''$  phase stabilizes in the entire bulk of the 9Sc1YbSZ crystals. Co-doping of the  $\text{ZrO}_2 - 9 \text{ mol.}\% \text{ Sc}_2\text{O}_3$  solid solutions with 1 mol.% ytterbia produces single-phase single crystals with the pseudocubic  $t''$  phase which is stable upon long-term air annealing.

Figure 3a shows the conductivity of the test crystals *vs* temperature in Arrhenius coordinates. Figure 3b shows the conductivity of the test crystals *vs*  $\text{Yb}_2\text{O}_3$  concentration.

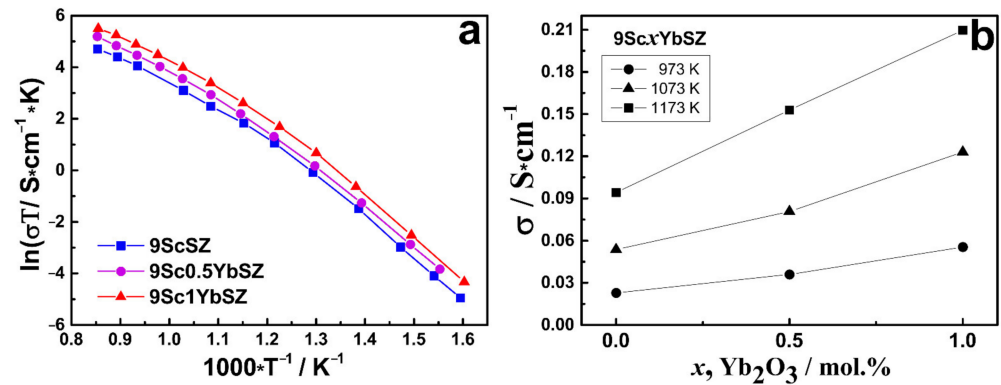


**Figure 3.** (a) Conductivity of test crystals *vs* temperature in Arrhenius coordinates and (b) Conductivity of test crystals *vs.*  $\text{Yb}_2\text{O}_3$  concentration.

As can be seen from Figure 3, the 9ScSZ crystals stabilized only with scandia have the lowest conductivity in the whole test temperature range. Co-doping of the crystals with 0.5 mol.%  $\text{Yb}_2\text{O}_3$  increases the ionic conductivity. Phase composition analysis showed that the as-grown 9Sc0.5YbSZ crystals contain the cubic phase along with the tetragonal phase and therefore their conductivity in the entire temperature range is higher than that of the tetragonal 9ScSZ crystals. The single-phase 9Sc1YbSZ crystals that contain the  $t''$  phase have the highest conductivity.

Figure 4 shows the conductivity of the as-grown and as-annealed crystals as a function of temperature.

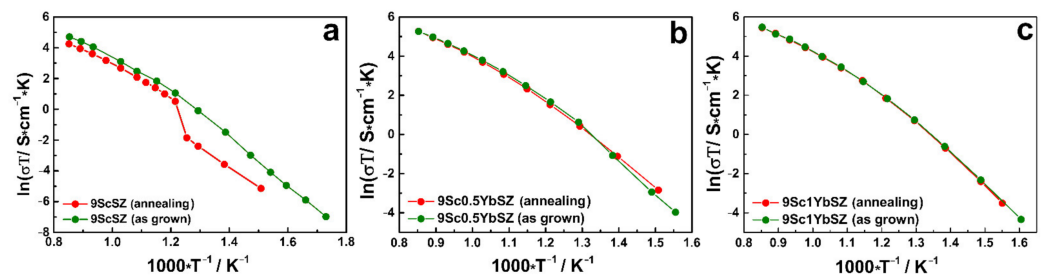


**Figure 4.** Conductivity of as-grown and as-annealed (a) 9ScSZ, (b) 9Sc0.5YbSZ, and (c) 9Sc1YbSZ crystals as a function of temperature.

The conductivity *vs* temperature curve of the as-annealed 9ScSZ crystal shows an abrupt increase in the conductivity at  $\sim 600^\circ\text{C}$  caused by the rhombohedral to cubic phase transition. The conductivity of the as-annealed 9Sc0.5YbSZ crystal decreases slightly. The conductivities of the as-grown and as-annealed 9Sc1YbSZ crystals are almost the same in the entire temperature range. Figure 5 shows the 1173 K conductivity of the as-grown and as-annealed crystals.

After air annealing at  $1000^\circ\text{C}$  for 400 h the 1173 K conductivity of the 9ScSZ crystal decreased by 35%, the 1173 K conductivity of the 9Sc0.5YbSZ crystal decreased by less than 10% and the 1173 K conductivity of the 9Sc1YbSZ crystal did not decrease.

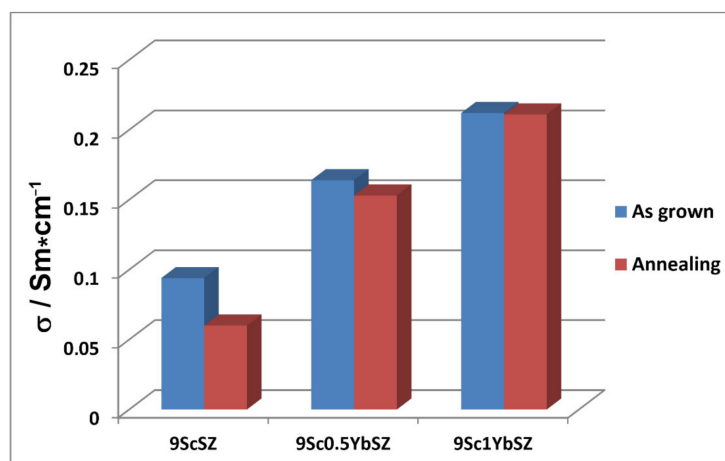


Figure 5. 1173 K conductivity of crystals as-grown and as-annealed at 1000 °C for 400 h.

#### 4. Summary

$(\text{ZrO}_2)_{0.91-x}(\text{Sc}_2\text{O}_3)_{0.09}(\text{Yb}_2\text{O}_3)_x$  solid solution crystals ( $x = 0; 0.005; 0.01$ ) were grown by directional melt crystallization in a cold crucible. The crystals were heat treated at 1000 °C for 400 h in air for determining the phase stability of the crystals and studying degradation of their conductivity.

The microstructure of the crystals was studied using polarized light optical microscopy for wafers cut along the growth axis. The 9ScSZ crystals that were stabilized only with scandia contained multiple twins in the entire bulk. The as-annealed 9ScSZ solid solutions contained larger structural features and microcracks in the bulk. Co-doping of the  $\text{ZrO}_2 - 9 \text{ mol.}\% \text{ Sc}_2\text{O}_3$  solid solutions with 0.5 mol.%  $\text{Yb}_2\text{O}_3$  produced discrete transparent regions in the crystals. However, the as-annealed 9Sc0.5YbSZ crystals were uniform and semitransparent and contained twins in the entire bulk. Co-doping of the  $\text{ZrO}_2 - 9 \text{ mol.}\% \text{ Sc}_2\text{O}_3$  solid solutions with 1 mol.%  $\text{Yb}_2\text{O}_3$  produced uniform and transparent single crystals. Annealing of the 9Sc1YbSZ crystals at the 1000 °C relieved the residual stress but the crystal remained transparent and did not contain twins.

The phase composition of the crystals was analyzed using X-ray diffraction and Raman spectroscopy. Co-doping of the  $\text{ZrO}_2 - 9 \text{ mol.}\% \text{ Sc}_2\text{O}_3$  solid solutions with ytterbia stabilized the annealing-stable high-temperature pseudocubic  $t''$  phase but the stabilization was only achieved at a co-doping oxide concentration of 1 mol.%. At lower  $\text{Yb}_2\text{O}_3$  concentrations the high-temperature phase stabilized but the cubic phase did not stabilize in the entire crystal bulk. In the 9Sc0.5YbSZ crystals, the content of the co-doping oxide is insufficient and after annealing the regions with the unstable cubic structure underwent a phase transition to the more stable tetragonal phase, and possibly part of the cubic phase transformed to the rhombohedral phase according to our Raman data.

Study of the transport properties of the crystals showed that the crystals stabilized only with scandia have the lowest conductivity in the entire test temperature range. Co-doping of the crystals with 0.5 mol.%  $\text{Yb}_2\text{O}_3$  increased their ionic conductivity. The single-phase 9Sc1YbSZ crystals that contained the  $t''$  phase had the highest ionic conductivity. Long-term high-temperature annealing did not reduce the ionic conductivity of the  $\text{ZrO}_2 - 9 \text{ mol.}\% \text{ Sc}_2\text{O}_3$  crystals co-doped with 1 mol%  $\text{Yb}_2\text{O}_3$ .

**Author Contributions:** Conceptualization, E.L. and N.T.; Formal analysis, V.M.; Investigation, A.K., G.K., I.K., N.L., F.M., V.M., N.S. and T.V.; Methodology, P.R.; Resources, A.K.; Supervision, E.L.; Validation, P.R. and N.T.; Visualization, A.K. and F.M.; Writing—review and editing, A.K., M.B., E.L., P.R. and N.T. All authors have read and agreed to the published version of the manuscript.

**Funding:** This research was funded by Russian Science Foundation, grant number 19-72-10113.

**Conflicts of Interest:** The authors declare no conflict of interest.

## References

1. Badwal, S.P.S.; Ciacchi, F.T.; Milosevic, D. Scandia–zirconia electrolytes for intermediate temperature solid oxide fuel cell operation. *Solid State Ionics* **2000**, *136*, 91–99. [[CrossRef](#)]
2. Kharton, V.V.; Marques, F.M.B.; Atkinson, A. Transport properties of solid oxide electrolyte ceramics: A brief review. *Solid State Ionics* **2004**, *174*, 135–149. [[CrossRef](#)]
3. Fergus, J.W. Electrolytes for solid oxide fuel cells. *J. Power Sources* **2006**, *162*, 30–40. [[CrossRef](#)]
4. Yokokawa, H.; Sakai, N.; Horita, T.; Yamaji, K.; Brito, M.E. Solid Oxide Electrolytes for High Temperature Fuel Cells. *Electrochemistry* **2005**, *73*, 20–30. [[CrossRef](#)]
5. Politova, T.I.; Irvine, J.T.S. Investigation of scandia–yttria–zirconia system as an electrolyte material for intermediate temperature fuel cells—influence of yttria content in system  $(Y_2O_3)_x(Sc_2O_3)_{(1-x)}(ZrO_2)_{89}$ . *Solid State Ionics* **2004**, *168*, 153–165. [[CrossRef](#)]
6. Jais, A.A.; Ali, S.A.M.; Anwar, M.; Somalu, M.R.; Muchtar, A.; Isahak, W.N.R.W.; Tan, C.Y.; Singh, R.; Brandon, N.P. Enhanced ionic conductivity of scandia-ceria-stabilized-zirconia (10Sc1CeSZ) electrolyte synthesized by the microwave-assisted glycine nitrate process. *Ceram. Int.* **2017**, *43*, 8119–8125. [[CrossRef](#)]
7. Zhang, J.; Lenser, C.; Menzler, N.H.; Guillon, O. Comparison of solid oxide fuel cell (SOFC) electrolyte materials for operation at 500 °C. *Solid State Ionics* **2020**, *344*, 115138. [[CrossRef](#)]
8. Abbas, H.A.; Argirusis, C.; Kilo, M.; Wiemhöfer, H.-D.; Hammad, F.F.; Hanafi, Z.M. Preparation and conductivity of ternary scandia-stabilised zirconia. *Solid State Ionics* **2011**, *184*, 6–9. [[CrossRef](#)]
9. Rocha, R.A.; Muccillo, E.N.S.; Dessemond, L.; Djurado, E. Thermal ageing of nanostructured tetragonal zirconia ceramics: Characterization of interfaces. *J. Eur. Ceram. Soc.* **2010**, *30*, 227–231. [[CrossRef](#)]
10. Hui, S.; Roller, J.; Yick, S.; Zhang, X.; Decès-Petit, C.; Xie, Y.; Maric, R.; Ghosh, D. A brief review of the ionic conductivity enhancement for selected oxide electrolytes. *J. Power Sources* **2007**, *172*, 493–502. [[CrossRef](#)]
11. Osiko, V.W.; Borik, M.A.; Lomonova, E.E. Synthesis of Refractory Materials by Skull Melting Technique. In *Springer Handbook of Crystal Growth*; Springer Science and Business Media LLC: Berlin/Heidelberg, Germany, 2010; pp. 433–477.
12. Kuz'minov, Y.S.; Lomonova, E.E.; Osiko, V.V. *Cubic Zirconia and Skull Melting*; Cambridge International Science Publishing Ltd.: Cambridge, UK, 2009; 346p.
13. Araki, W.; Hanashiro, D.; Arai, Y.; Malzbender, J. Fracture mechanism of scandia-doped zirconia. *Acta Mater.* **2013**, *61*, 3082–3089. [[CrossRef](#)]
14. Fujimori, H.; Yashima, M.; Kakihana, M.; Yoshimura, M. Structural Changes of Scandia-Doped Zirconia Solid Solutions: Rietveld Analysis and Raman Scattering. *J. Am. Ceram. Soc.* **2005**, *81*, 2885–2893. [[CrossRef](#)]
15. Simoncic, P.; Navrotsky, A. Systematics of Phase Transition and Mixing Energetics in Rare Earth, Yttrium, and Scandium Stabilized Zirconia and Hafnia. *J. Am. Ceram. Soc.* **2007**, *90*, 2143–2150. [[CrossRef](#)]
16. Spirin, A.; Ivanov, V.; Nikonov, A.; Lipilin, A.; Paranin, S.; Khrustov, V.; Spirina, A. Scandia-stabilized zirconia doped with yttria: Synthesis, properties, and ageing behavior. *Solid State Ionics* **2012**, *225*, 448–452. [[CrossRef](#)]
17. Tataryn, T.; Savytskii, D.; Paulmann, C.; Bismayer, U. Twin structure of the  $ZrO_2:Sc_2O_3$  crystal. *Radiat. Phys. Chem.* **2009**, *78*, S101–S104. [[CrossRef](#)]
18. Omar, S.; Bin Najib, W.; Chen, W.; Bonanos, N. Electrical Conductivity of 10 mol%  $Sc_2O_3$ -1 mol%  $M_2O_3$ - $ZrO_2$  Ceramics. *J. Am. Ceram. Soc.* **2012**, *95*, 1965–1972. [[CrossRef](#)]
19. Araki, W.; Koshikawa, T.; Yamaji, A.; Adachi, T. Degradation mechanism of scandia-stabilised zirconia electrolytes: Discussion based on annealing effects on mechanical strength, ionic conductivity, and Raman spectrum. *Solid State Ionics* **2009**, *180*, 1484–1489. [[CrossRef](#)]
20. Badwal, S.; Drennan, J. Microstructure/conductivity relationship in the scandia-zirconia system. *Solid State Ionics* **1992**, *53–56*, 769–776. [[CrossRef](#)]
21. Nomura, K.; Mizutani, Y.; Kawai, M.; Nakamura, Y.; Yamamoto, O. Aging and Raman scattering study of scandia and yttria doped zirconia. *Solid State Ionics* **2000**, *132*, 235–239. [[CrossRef](#)]
22. Haering, C.; Roosen, A.; Schichl, H.; Schnoller, M. Degradation of the electrical conductivity in stabilised zirconia system Part II: Scandia-stabilised zirconia. *Solid State Ionics* **2005**, *176*, 261–268. [[CrossRef](#)]
23. Yamamoto, O.; Arati, Y.; Takeda, Y.; Imanishi, N.; Mizutani, Y.; Kawai, M.; Nakamura, Y. Electrical conductivity of stabilized zirconia with ytterbia and scandia. *Solid State Ionics* **1995**, *79*, 137–142. [[CrossRef](#)]
24. Zhigachev, A.O.; Zhigacheva, D.V.; Lyskov, N.V. Influence of yttria and ytterbia doping on phase stability and ionic conductivity of ScSZ solid electrolytes. *Mater. Res. Express* **2019**, *6*, 105534. [[CrossRef](#)]
25. Kulebyakin, A.V.; Borik, M.A.; Kuritsyna, I.E.; Larina, N.A.; Lomonova, E.E.; Milovich, F.O.; Myzina, V.A.; Ryabochkina, P.A.; Skryleva, E.A.; Tabachkova, N.Y.; et al. Structural characteristics of melt-grown  $(ZrO_2)_{0.99}(Sc_2O_3)(Yb_2O_3)_{0.01}$  solid solution crystals and their effect on ionic conductivity. *J. Cryst. Growth* **2020**, *547*, 125808. [[CrossRef](#)]
26. Agarkov, D.A.; Borik, M.A.; Bredikhin, S.I.; Burmistrov, I.N.; Eliseeva, G.M.; Kulebyakin, A.V.; Kuritsyna, I.E.; Lomonova, E.E.; Milovich, F.O.; Myzina, V.A.; et al. Phase compositions, structures and properties of scandia-stabilized zirconia solid solution crystals co-doped with yttria or ytterbia and grown by directional melt crystallization. *Solid State Ionics* **2020**, *346*, 115218. [[CrossRef](#)]
27. Shukla, V.; Singh, S.; Subramaniam, A.; Omar, S. Long-Term Conductivity Stability of Metastable Tetragonal Phases in  $1Yb_2O_3-xSc_2O_3-(99-x)ZrO_2$  ( $x = 7, 8$  mol %). *J. Phys. Chem. C* **2020**, *124*, 23490–23500. [[CrossRef](#)]

28. Yashima, M. Metastable-stable phase diagrams in the zirconia-containing systems utilized in solid-oxide fuel cell application. *Solid State Ionics* **1996**, *86*, 1131–1149. [[CrossRef](#)]
29. Sheu, T.-S.; Xu, J.; Tien, T.-Y. Phase Relationships in the ZrO<sub>2</sub>-Sc<sub>2</sub>O<sub>3</sub> and ZrO<sub>2</sub>-In<sub>2</sub>O<sub>3</sub> Systems. *J. Am. Ceram. Soc.* **1993**, *76*, 2027–2032. [[CrossRef](#)]
30. Ingel, R.P.; Iii, D.L. Lattice Parameters and Density for Y<sub>2</sub>O<sub>3</sub>-Stabilized ZrO<sub>2</sub>. *J. Am. Ceram. Soc.* **1986**, *69*, 325–332. [[CrossRef](#)]
31. Merle, T.; Guinebretiere, R.; Mirgorodsky, A.; Quintard, P. Polarized Raman spectra of tetragonal pure ZrO<sub>2</sub> measured on epitaxial films. *Phys. Rev. B* **2002**, *65*, 144302. [[CrossRef](#)]
32. Borik, M.A.; Volkova, T.V.; Kulebyakin, A.V.; Lomonova, E.E.; Milovich, F.O.; Myzina, V.A.; Osiko, V.V.; Ryabochkina, P.A.; Tabachkova, N.Y.; Uslamina, M.A.; et al. Nanostructured crystals of partially yttria-stabilized and Nd<sup>3+</sup> doped zirconia: Structure and luminescent properties. *J. Alloy. Compd.* **2015**, *621*, 295–300. [[CrossRef](#)]
33. Hemberger, Y.; Wichtner, N.; Berthold, C.; Nickel, K.G. Quantification of Yttria in Stabilized Zirconia by Raman Spectroscopy. *Int. J. Appl. Ceram. Technol.* **2015**, *13*, 116–124. [[CrossRef](#)]
34. Yashima, M.; Sasaki, S.; Kakihana, M.; Yamaguchi, Y.; Arashi, H.; Yoshimura, M. Oxygen-induced structural change of the tetragonal phase around the tetragonal–cubic phase boundary in ZrO<sub>2</sub>-YO<sub>1.5</sub> solid solutions. *Acta Crystallogr. Sect. B Struct. Sci.* **1994**, *50*, 663–672. [[CrossRef](#)]